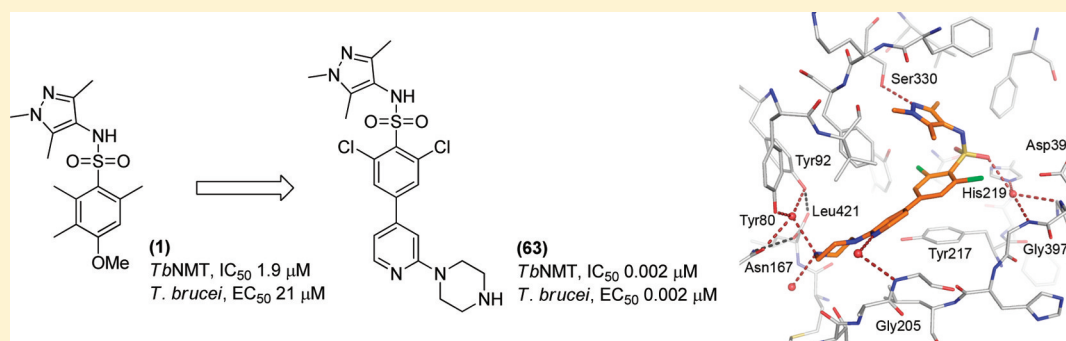


Discovery of a Novel Class of Orally Active Trypanocidal *N*-Myristoyltransferase Inhibitors

Stephen Brand, Laura A. T. Cleghorn, Stuart P. McElroy, David A. Robinson, Victoria C. Smith, Irene Hallyburton, Justin R. Harrison, Neil R. Norcross, Daniel Spinks, Tracy Bayliss, Suzanne Norval, Laste Stojanovski, Leah S. Torrie, Julie A. Frearson, Ruth Brenk, Alan H. Fairlamb, Michael A. J. Ferguson, Kevin D. Read, Paul G. Wyatt, and Ian H. Gilbert*

Drug Discovery Unit, Division of Biological Chemistry and Drug Discovery, College of Life Sciences, University of Dundee, Sir James Black Centre, Dundee, DD1 5EH, U.K.

S Supporting Information



ABSTRACT: *N*-Myristoyltransferase (NMT) represents a promising drug target for human African trypanosomiasis (HAT), which is caused by the parasitic protozoa *Trypanosoma brucei*. We report the optimization of a high throughput screening hit (1) to give a lead molecule DDD85646 (63), which has potent activity against the enzyme ($IC_{50} = 2$ nM) and *T. brucei* ($EC_{50} = 2$ nM) in culture. The compound has good oral pharmacokinetics and cures rodent models of peripheral HAT infection. This compound provides an excellent tool for validation of *T. brucei* NMT as a drug target for HAT as well as a valuable lead for further optimization.

INTRODUCTION

Human African trypanosomiasis (HAT) or sleeping sickness is caused by two subspecies of the protozoan parasite *Trypanosoma brucei* (*T. brucei gambiense* and *T. b. rhodesiense*), which are transmitted by the bite of an infected tsetse fly. The disease, which is fatal unless treated, has two stages: an initial peripheral infection during which the parasites are found in the bloodstream and gives rise to nonspecific symptoms; a second stage when parasites enter the central nervous system, causing the classic symptoms of HAT, eventually leading to coma and death. Currently there are five treatments available, although none of them are satisfactory because of toxicity, treatment failures, and the requirement for parenteral administration, which is inappropriate in a rural African setting.¹

The enzyme *N*-myristoyltransferase (NMT) represents a promising drug target, since its essentiality has been demonstrated in many organisms. Moreover, in *T. brucei*, RNAi knockdown of NMT has been shown to be lethal in cell culture and to abrogate infectivity in a mouse model of infection.^{2,3}

NMT catalyzes the co-translational transfer of myristate from myristoyl-CoA to the N-terminal glycine of a subset of

eukaryotic proteins, a modification that has been implicated in subcellular targeting to membrane locations and/or activation and stabilization of the substrate protein (Figure 1).⁴ While there is an incomplete knowledge of the targets of NMT in *T. brucei* and their subsequent downstream effects, bioinformatic analysis suggests there are in excess of 60 potential substrates,² two of which (ADP-ribosylation factor-1 protein (ARF-1) and ADP-ribosylation factor-like protein (ARL-1)) have been characterized and shown to be essential for bloodstream parasite viability.⁵ Therefore, inhibition of the enzyme would be expected to have pleiotropic effects through its potential to affect multiple pathways.

The enzyme operates via a Bi-Bi mechanism in which binding of myristoyl-CoA induces a conformational rearrangement that reveals the peptide binding site.² The myristate group is then transferred in a nucleophilic addition–elimination reaction, which is followed by sequential release of CoA followed by the myristoylated protein. Several industrial research groups have targeted NMT from the yeast *Candida albicans*, initially

Received: August 14, 2011

Published: December 7, 2011

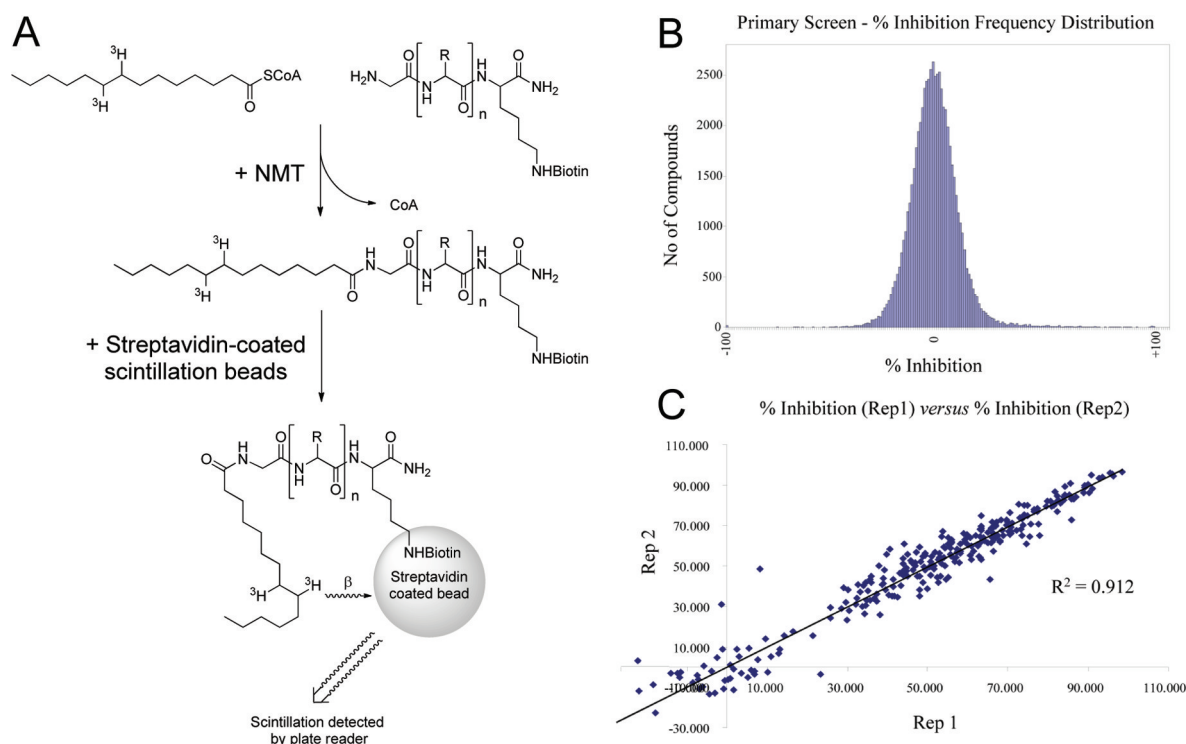


Figure 1. Format and performance of the HTS assay: (A) % inhibition and IC_{50} values determined using a scintillation proximity assay;² (B) frequency histogram representing % inhibition values for the HTS. Hits are designated as those compounds that displayed a % inhibition equal to or greater than 3 standard deviation units above the mean (40% inhibition). (C) Comparison of replicate % inhibition values for the 352 primary screen hits.

developing peptidomimetic inhibitors,^{6–10} which had limited cellular activity. More recently promising small molecule inhibitors, based around benzofuran^{11–14} and benzothiazole^{15,16} cores, have been discovered.² Development of these compounds as antifungal agents has not been continued presumably because of the inability to derive compounds with broad-spectrum antifungal activity.

We have previously reported biological studies that demonstrate the validity of *T. brucei* NMT (*Tb*NMT) as a druggable target for HAT, using the prototypic *Tb*NMT inhibitor DDD85646 (**63**).^{17,18} In this paper, we describe the medicinal chemistry that led to the discovery of this key inhibitor.

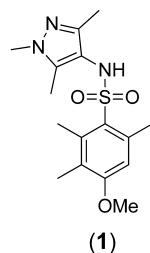
RESULTS AND DISCUSSION

Hit Discovery. *Tb*NMT entered our discovery portfolio for HAT following a positive assessment of its potential as a drug target, according to our published criteria.¹⁹ When the project commenced, there was a clinical need for safe oral drugs active in the first acute stage of the disease, in addition to the most favored profile of activity in both stages of HAT. Consequently, there was not an absolute requirement for compounds to access the CNS, relaxing some of the criteria required for compound progression, for example, polar surface area (PSA). Screening of a selection of antifungal compounds against *Tb*NMT (a repositioning or piggy-back approach⁴) by Smith and colleagues at the University of York, U.K., failed to identify substantially potent or druglike compounds.²⁰ Similarly we did not observe significant inhibition of *Tb*NMT with the potential benzofuran leads RO-09-4609¹³ and RO-09-4879¹³ (see Supporting Information), or related analogues, originally developed by Roche against the fungal species *C. albicans*. Subsequently,

comparison of X-ray crystal structures has revealed that there are substantial differences between the *C. albicans* NMT structure and that of NMT from *Leishmania major*. The *T. brucei* NMT enzyme (for which there is no structure to date) is most closely related to that of the *L. major* enzyme (74% sequence identity overall, 94% sequence identity within the active site).

In the absence of any reported tractable chemical start points, we opted to carry out a high-throughput screen (HTS) using our 63362-compound diversity library.²¹ A convenient homogeneous scintillation–proximity based assay in 384-well plate format was used to screen compounds, which employed *Tb*NMT, tritiated myristoyl-CoA, the biotinylated peptide CAP5.5²² (sequence GCGGSKVKPQQPPQAK), and streptavidin coated polyvinyltoluene scintillation beads (Figure 1). Compounds were initially screened in singlicate at 30 μ M, and the screen performance was excellent, with a mean (\pm SD) Z' = 0.79 ± 0.05 ($n = 210$ plates). Compounds showing greater than 50% inhibition were reconfirmed in duplicate, and then potency was determined via 10-point half-log dilution curves (30 μ M to 1.5 nM). Hit compounds shown to nonspecifically inhibit the assay signal were eliminated from further evaluation. Key compounds were also screened against human NMT-1 (*Hs*NMT-1) and against the bloodstream form of the *T. b. brucei* (BSF427, VSG118) parasite in culture. Inhibition of proliferation of human MRC5 cells was used as an initial toxicity counterscreen (see Experimental Section).

Optimization of the Pyrazole Sulfonamides. Of the compounds confirmed as validated hits by testing of resynthesized material, we opted to focus our attention on compound **1** (Figure 2), the most potent example of a series of nine *N*-pyrazole arylsulfonamides identified by the HTS.



(1)
*Tb*NMT, IC₅₀ 1.9 μM
*Hs*NMT-1, IC₅₀ 22 μM
T. brucei, EC₅₀ 21 μM
 MRC5, EC₅₀ 55 μM

Figure 2. Structure and biological activity of compound **1**.

The compound had potencies of 1.9 and 22 μM against *Tb*NMT and *Hs*NMT-1, respectively, demonstrating encouraging selectivity over the human isoform while having promising ligand efficiency (LE = 0.34).²³ Moreover, **1** had moderate activity against the parasite *in vitro* (EC₅₀ = 21 μM). Testing of **1** against varying concentrations of substrate peptide indicated that it is competitive for substrate binding and hence binds to the peptide binding site. Thus, changing the concentration of CAP5.5 from 0.5 to 16 μM caused the IC₅₀ for *Tb*NMT to change from 1.0 to 4.3 μM, as previously described.¹⁷

In the absence of any structural information for *Tb*NMT to guide rational inhibitor design, we adopted a pragmatic chemistry-driven approach through which we aimed to (i) understand the importance for binding of existing parts of the inhibitor with a view to optimizing these and (ii) identify appropriate positions from which to extend the molecule and seek further ligand–protein interactions that improve affinity. A systematic program was therefore carried out to define the key pharmacophoric features of **1**. A common requirement for high potency in previously reported NMT inhibitors is a basic functionality that interacts electrostatically with the C-terminal carboxylic acid of NMT, in the region of the active site normally occupied by the amino group of the peptide substrate's terminal glycine. Although the binding mode of **1** was unknown from the outset, we anticipated that incorporation of a basic center in an appropriate location would significantly enhance potency of the hits, as experienced by previous NMT inhibitor programs.^{7–14,16,17,24}

Investigation of SAR at the Pyrazole Group. Initially we investigated changes around the pyrazole of **1** (Table 1). Compounds were prepared by reaction of an amine with 3-methoxy-2,4,5-trimethylbenzenesulfonyl chloride. The pyrazole N-substituent could be modified by using a standard alkylation reaction on the symmetrical intermediate (**2**) (Scheme 1).

Removal of the *N*-methyl substituent of **1** (**2**) and replacement of the *N*-methyl substituent with a larger *n*-propyl (**3**) or isopropyl (**4**) group significantly reduced activity. A number of potential aromatic replacements of the pyrazole, including imidazopyridine (**7**), pyridine (**8**), substituted pyridine (**9**), isoxazole (**10** and **11**), phenyl (**12**), and benzyl (**13**) together with addition of a methylene between the sulfonamide and the pyrazole (**14**), were investigated. The only replacements that gave some potency were the 2-methylpyridyl derivative **9** (IC₅₀ = 10 μM) and the isoxazole derivative **10** (IC₅₀ = 19 μM), although these were both less potent than the original *N*-methylpyrazole **1** (IC₅₀ = 1.9 μM). In combination, these results implied that the pyrazole N2 nitrogen was

Table 1. Activities of Pyrazoles and Pyrazole Replacements against *Tb*NMT^a

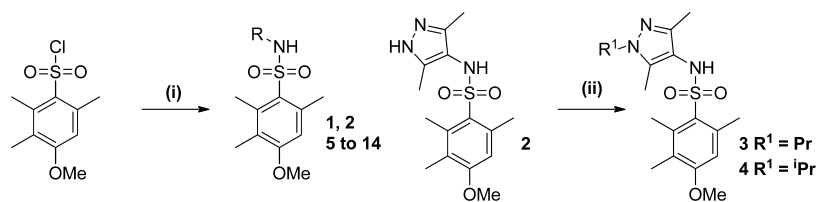
No.	R	<i>Tb</i> NMT IC ₅₀ (μM)	No.	R	<i>Tb</i> NMT IC ₅₀ (μM)
1		1.9	8		>100
2		>100	9		10
3		28	10		19
4		>100	11		>100
5		>100	12		>100
6		>100	13		>100
7		>100	14		>100

^aIC₅₀ values are shown as mean values of two or more determinations. Standard deviation is typically within 2-fold from the IC₅₀.

interacting with the enzyme as a hydrogen bond acceptor, since removal of it (e.g., **12**) or increasing steric bulk around it (**3** and **4**) caused marked reductions in potency. Only isoelectronic heterocycles **9** and **10**, with a similarly located hydrogen bonding acceptor capability, retained activity. Therefore, the trimethylpyrazole moiety of **1** was retained in further studies.

Investigation of SAR at the Sulfonamide Group. A series of analogues were made to investigate changes at the sulfonamide linker of compound **15** (Table 2). These were prepared as described in Scheme 2. In general, amides and sulfonamides were prepared by reaction of the appropriate amine with a benzoyl chloride or sulfonyl chloride, respectively.

Replacement of the sulfonamide of **15** with an amide (**17**) as well as reversing the sulfonamide (**19**) and amide (**24**) led to a loss of activity. This suggests that either both sulfonamide oxygen atoms are involved in binding, or the sulfonamide causes a conformational effect important for locating the pyrazole ring relative to the aromatic system. It is known from crystallographic studies that *N*-substituted sulfonamides prefer to adopt a “kinked” conformation with substituents on the same side of the S–N bond.²⁵ Therefore, amide **17** was *N*-substituted (**18**) with the aim of forcing the amide into a similar *cis*-conformation, but this compound was also inactive. Similarly, using an amine (**21**) or ether (**22**) as a linker led to a reduction in activity, presumably due

Scheme 1^a

^aReagents: (i) NH₂R, pyridine; (ii) R¹Br, Cs₂CO₃, DMF.

Table 2. Activities of Sulfonamide Replacements against *Tb*NMT^a

No.	Compound	<i>Tb</i> NMT IC ₅₀ (μM)	No.	Compound	<i>Tb</i> NMT IC ₅₀ (μM)
15		14	20		42
16		10	21		>100
17		> 100	22		>100
18		> 100	23		>100
19		>100	24		>100

^aIC₅₀ values are shown as mean values of two or more determinations. Standard deviation is typically within 2-fold from the IC₅₀.

to their greater flexibility and/or loss of hydrogen bond acceptor capability. Addition of an extra methylene (**23**) caused a loss of activity. Only the sulfone replacement (**20**) showed some activity (IC₅₀ = 42 μM), although this was less than the corresponding sulfonamide (**15**).

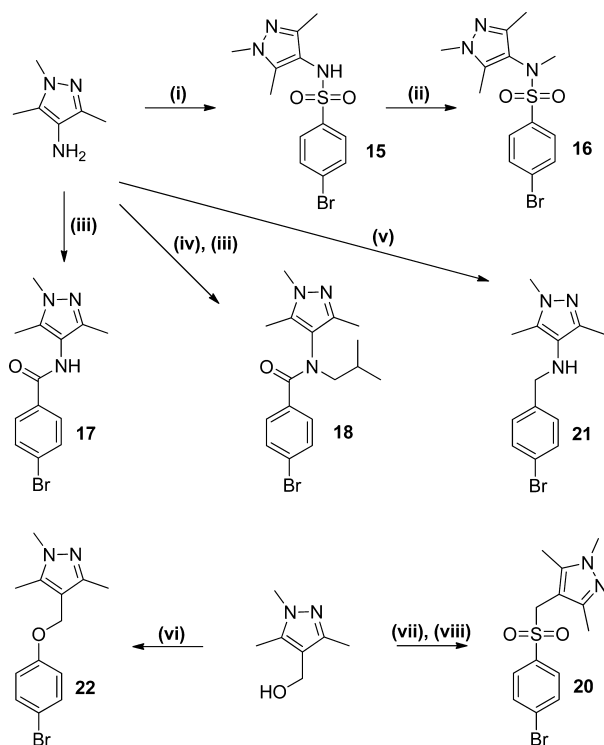
The sulfonamide could be N-methylated with little effect on activity (**16**), suggesting that the sulfonamide NH group is not a participant in a significant interaction with *Tb*NMT. Further substitution of the sulfonamide nitrogen of a related compound (**29**) with a variety of simple alkyl groups, while not unduly detrimental, did not significantly enhance activity (see Table S1 in the Supporting Information), with potencies observed in the range of 0.5 μM (R = methyl) to 9.3 μM (R = CH₂C≡CCH₃).

Investigation of SAR at the Aryl Group. An investigation of diverse substitutions of the arylsulfonyl ring was carried out. Compounds were prepared using parallel synthesis techniques (Scheme 3). We initially prepared 60 analogues (see Table S2 in the Supporting Information); key compounds are shown in Table 3.

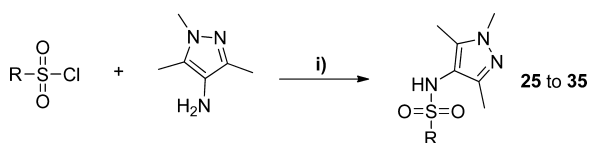
In general, we found SAR around the ring to be comparatively flat, with even relatively sterically demanding substitutions in ortho-, meta-, and particularly para-positions tolerated, albeit without significant enhancements in potency. Given the largely inconsequential effect on potency of groups around the aromatic ring and the ability to tolerate even large substituents (e.g., **31**, IC₅₀ = 1.9 μM), we speculated that these

substituents occupy a “sequence insensitive” region of the active site (i.e., the region that accommodates residues 2–4 of the substrate peptide), which is known to be capable of binding a variety of residues but to favor hydrophobic residues.^{26,27} Given the approximately 10-fold improvement in activity obtained with the 2,6-dichloro substitution of **28** (IC₅₀ = 1.0 μM) compared with **25** (IC₅₀ = 12 μM), we continued to search for improvements in activity using this framework and utilized compound **29** in a Suzuki reaction for the preparation of a small speculative library of biaryl derivatives (see Table S3 in the Supporting Information). Of the 14 analogues prepared, only **36** (IC₅₀ = 0.9 μM) had activity comparable to that of **29**.

Additional Protein–Ligand Interactions from an Aminopyridine Scaffold. Since relatively bulky substitution was best tolerated in the para-position of the sulfonamide aromatic system (e.g., **36**), we thought it most appropriate to seek additional protein–ligand interactions by probing from this position. The aminopyridyl moiety did not appear to be detrimental to binding per se (e.g., **31**, IC₅₀ = 1.9 μM); therefore, an additional exploratory library of 44 compounds was produced using a nucleophilic aromatic substitution reaction between chloropyridine **37** and a diverse set of commercially available amines (Scheme 4). Selected compounds are shown in Table 4 (full data can be seen in Table S4 in the Supporting Information).

Scheme 2^a

^aReagents: (i) 4-bromobenzenesulfonyl chloride, pyridine, DCM; (ii) MeI, Cs₂CO₃, DMF; (iii) 4-bromobenzoyl chloride, pyridine, DCM; (iv) isobutyraldehyde, AcOH, NaBH(OAc)₃, DCM, 0 °C → room temp; (v) 4-bromobenzyl bromide, K₂CO₃, KI, DMF; (vi) diisopropyl azodicarboxylate, polymer supported PPh₃, pyridine, DCM; (vii) SOCl₂, chloroform; (viii) sodium 4-bromobenzene sulfinate, H₂O, acetone.

Scheme 3^a

^aReagents: (i) pyridine, DCM.

Again, a variety of substituents were tolerated, but with flat SAR, with activity generally in the low micromolar range. However, two compounds were particularly noteworthy because of the striking difference in potency despite their structural similarity. Compounds **41** (IC₅₀ = 38 μM) and **42** (IC₅₀ = 0.14 μM) differ only in having a morpholine or a methylpiperazine at the terminus of an ethyl linkage. We attributed the greater potency of **42** to its potential to form an electrostatic interaction via the protonatable terminal amine, since this approximately 100-fold improvement in activity is consistent with formation of a ligand–protein salt bridge, typically worth 10–400 kJ/mol. This interaction would not be possible via the morpholine of **41**. We subsequently demonstrated through surrogate crystallographic studies in *Lm*NMT that this is the most probable explanation for the increase in activity against *Tb*NMT (see Structural Studies). Furthermore, replacement of the basic terminal nitrogen of **42** with a methylene (i.e., **44**, IC₅₀ = 14 μM) gave a large drop in activity, consistent with our reasoning. Given that enzyme kinetic studies using **1** indicated that this series binds in the peptide

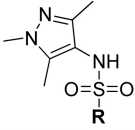
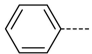
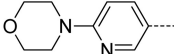
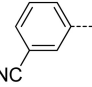
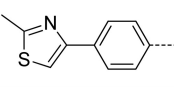
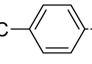
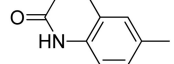
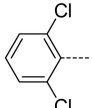
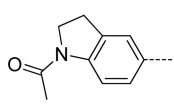
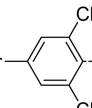
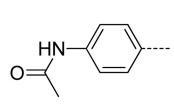
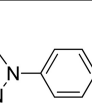
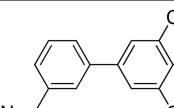
binding site, we speculated that **42** forms a salt bridge with the carboxyl group of the terminal residue of *Tb*NMT (Val446), a mechanistically vital residue for myristoyl transfer. Moreover, this is an interaction that is found with all currently known inhibitors of NMT that have very high potency.^{6–16}

An important objective of target-based discovery programmes is to achieve compounds with high selectivity against relevant human isoforms in order to minimize the risk of target-driven toxicity. While there is a high degree of sequence similarity between *Tb*NMT and *Hs*NMT-1 and -2 (41% identity, 69% similarity vs *Hs*NMT-1; 44% identity, 68% similarity vs *Hs*NMT-2) particularly at the active site (83% identity, 90% similarity vs both isoforms), fortuitously key compounds demonstrate upward of 60-fold selectivity against *Hs*NMT-1 (e.g., **42**).

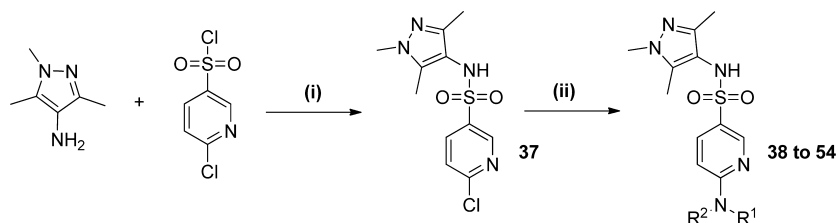
A number of interesting observations were made when we further investigated a variety of analogues with pendent amines (Table 4). Differences in pK_a (calculated using ACDlabs software, version 11.02) might account for the greater potency of the piperidine analogue **47** (IC₅₀ = 0.03 μM; pK_a = 9.6), which is 4-fold more active than the analogous piperazine **42** (IC₅₀ = 0.14 μM; pK_a = 7.9), and the lower potency of imidazole **50** (IC₅₀ = 1.3 μM; pK_a = 7.1). We were somewhat surprised that imidazole proved to be a poor substitute for an alkylamine, since this finding is in contrast to that of Searle.⁷ The *des*-methylpiperazine **43** (IC₅₀ = 1.0 μM; pK_a = 9.3), which we would expect to be more basic and therefore more potent, was actually around 8-fold less active than **42** potentially because of loss of a hydrophobic interaction at the terminal methyl group. Moreover, the loss of this methyl group causes a reduction in selectivity against *Hs*NMT-1 compared to **42** (16-fold vs more than 60-fold). The spacer length to the amine could be varied; compare the two-carbon linker of **42** (IC₅₀ = 0.14 μM) with the three-carbon linker of **49** (IC₅₀ = 0.11 μM). However, the linker length in compound **46** (IC₅₀ = 2.1 μM) would appear to be too short to optimally form the key interaction with the terminal nitrogen. There were indications that the orientation of the amine has an effect on activity (for example, compare conformationally constrained analogues **51**, IC₅₀ = 0.11 μM, **52**, IC₅₀ = 0.03 μM, and **40**, IC₅₀ = 0.36 μM) in compounds where the amines are constrained in slightly different orientations. Whereas methylation of the terminal nitrogen appears to be beneficial for activity, higher substitution, i.e., with isopropyl (**45**), phenyl (**48**), benzyl (**53**) or *tert*-butyloxycarbonyl groups (**54**), was not tolerated.

Effect of Conformational Restraint on the Activity of 42. Having identified a key protein–ligand electrostatic interaction in compounds typified by the prototype **42**, we continued to explore the concept of using conformational restraint to orient the amine in an optimal manner to increase potency. We chose to revisit the biaryl system of **36** as a suitable scaffold from which to attach an amine moiety because it conveyed the dual benefits of an unambiguous conformation combined with the potency-enhancing effect of the 2,6-dichlorophenyl moiety. A series of compounds was examined where a protonatable nitrogen was attached in various positions around the distal aryl ring (Table 5). Biaryl compounds **56**, **59**, **60**, and **63** could be prepared using a Suzuki cross-coupling reaction of commercially available arylboronic acids or esters with **29**, as the key step (Scheme 5). Alternatively, **29** could be converted to the corresponding pinacolboronic ester by cross-coupling with bispinacolatodiboron, allowing Suzuki reaction in the reverse sense with the appropriate commercially available

Table 3. Activities of Aryl Replacements against *Tb*NMT^a

					
No.	R	<i>Tb</i> NMT IC ₅₀ (μM)	No.	R	<i>Tb</i> NMT IC ₅₀ (μM)
25		12	31		1.9
26		28	32		12
27		32	33		3.3
28		1.0	34		8.6
29		0.34	35		2.8
30		4.8	36		0.9

^aIC₅₀ values are shown as mean values of two or more determinations. Standard deviation is typically within 2-fold from the IC₅₀.

Scheme 4^a

^aReagents: (i) pyridine, DCM; (ii) HNR¹R², EtOH, 130–155 °C.

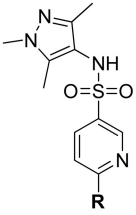
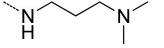
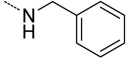
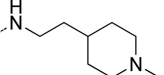
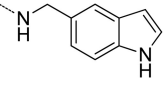
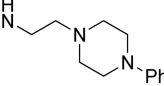
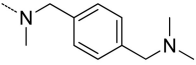
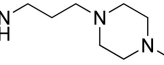
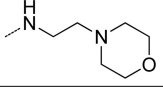
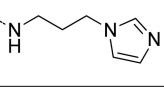
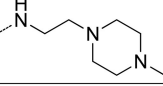
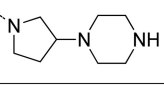
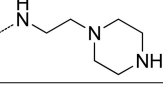
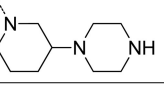
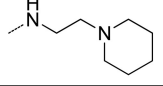
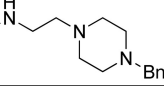
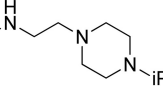
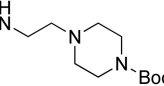
aryl bromide. Benzylamine compounds **57**, **58**, **61**, and **62** were prepared by reductive amination of benzaldehyde **55**.

It is clear from these variations that substituents in the meta-position consistently gave significantly higher potency than those in the para-position; for example, compare **57** (IC₅₀ = 1.2 μM) with **61** (IC₅₀ = 0.005 μM); **58** (IC₅₀ = 11 μM) with **62** (IC₅₀ = 0.02 μM); and **59** (IC₅₀ = 0.29 μM) with **63** (IC₅₀ = 0.002 μM). A notable feature of compound **63**, the most potent of these constrained molecules, is that it also potently inhibits the human isoform of NMT (*Tb*NMT IC₅₀ = 0.002 μM vs *Hs*NMT-1 IC₅₀ = 0.003 μM). In addition, DDD85646 also significantly inhibits the *N*-myristoyltransferase of other species, including *Leishmania major* (*Lm*NMT IC₅₀ = 0.002 μM) and *Trypanosoma cruzi* (*Tc*NMT IC₅₀ = 0.003 μM), which suggests that this compound has potential utility as a lead for other infectious diseases.

Pharmacology of 63. The intravenous (3 mg/kg) and oral (10 mg/kg) pharmacokinetics of **63** have been assessed in the female NMRI mouse, the species and strain used in the acute animal model of HAT. Compound **63** has low blood clearance (Cl_b = 6 mL min⁻¹ kg⁻¹) and low volume of distribution (V_d = 0.4 L/kg) with moderate half-life (t_{1/2} = 1.2 h) and oral bioavailability (F = 19%). Compound **63** (DDD85646) as the hydrochloride salt has high aqueous solubility (>15 mg/mL) and an appreciable unbound fraction in mouse and human plasma (11% and 18%, respectively).¹⁷

The pharmacokinetic properties of **63** therefore have enabled twice a day oral dosing, at a tolerated level, to achieve high exposure of free drug relative to the EC₉₀ for parasite proliferation, making it a useful tool compound for validating the target in the animal model of acute HAT. In this model, the mice are infected with parasites and then treated with compound **3** days later for 4 days. After treatment mice are

Table 4. Activities of Aryl Replacements against *Tb*NMT and *Hs*NMT-1^a

							
No.	R	<i>Tb</i> NMT IC ₅₀ (μM)	<i>Hs</i> NMT-1 IC ₅₀ (μM)	No.	R	<i>Tb</i> NMT IC ₅₀ (μM)	<i>Hs</i> NMT-1 IC ₅₀ (μM)
37	Cl	26	>100	46		2.1	n.d.
38		1.3	17	47		0.03	1.0
39		0.33	2.7	48		>1	>1
40		0.36	n.d.	49		0.11	2.4
41		38	n.d.	50		1.3	8.7
42		0.14	8.2	51		0.11	1.6
43		1.0	16	52		0.03	0.11
44		14	74	53		>10	>10
45		>1	>1	54		>10	>10

^aIC₅₀ values are shown as mean values of two or more determinations. Standard deviation is typically within 2-fold from the IC₅₀. n.d. = not determined.

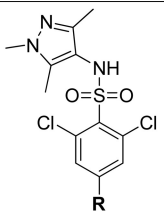
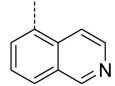
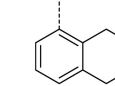
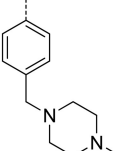
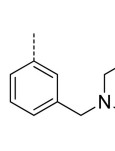
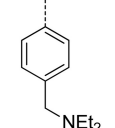
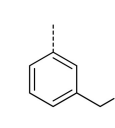
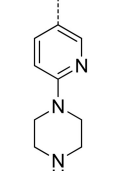
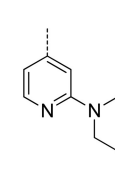
monitored for levels of parasitemia. Cure is defined as mice showing no signs of parasitemia 30 days after infection. The Kaplan–Meier survival plot for female NMRI mice ($n = 5$ per dose group) after infection with *T. b. brucei* s427 (inoculum 1×10^4 parasites) following oral treatment with **63** has been described previously.¹⁷ The minimal orally efficacious dose was found to be 12.5 mg/kg b.i.d. for 4 days. In contrast, the minimal orally efficacious dose in the more refractory but clinically relevant *T. b. rhodesiense* model of HAT was 50 mg/kg b.i.d. for 4 days.¹⁷ This reduced sensitivity *in vivo* is not due to reduced sensitivity of the compound *in vitro* but may be a result of the known precedent for this species to occupy privileged sites *in vivo*.¹⁷

Unfortunately, **63** has restricted brain penetration (brain/blood ratio of <0.1), consistent with its physicochemical properties (PSA = 92, MW = 495). Moreover, **63** also appears to be a weak P-glycoprotein substrate as evidenced by the Caco-2 efflux ratio (5.4) and the 3-fold increase in brain/blood ratio observed in rat when the P-glycoprotein inhibitor GF120918²⁸ is co-administered, which at least partially explains the lack of CNS penetration. The low concentration of **63**

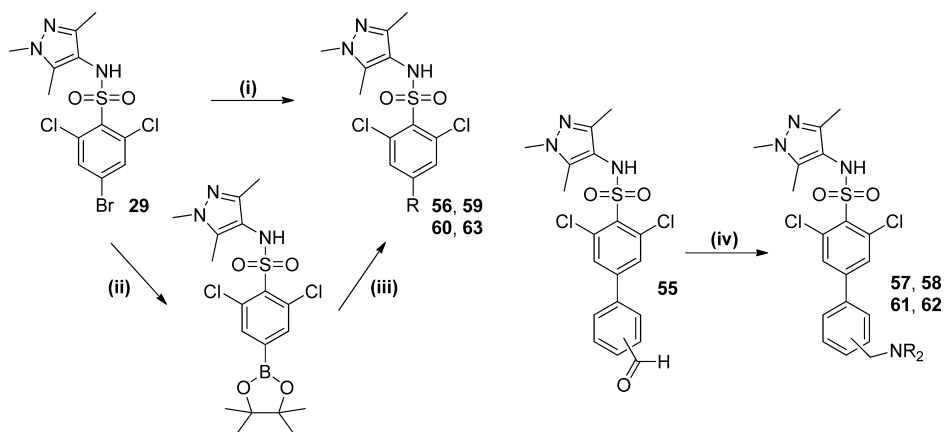
measured in brain might simply represent residual compound present in the intravascular volume. That said, given its high potency, **63** was progressed to a stage 2 HAT efficacy study at the maximum tolerated dose (100 mg/kg po b.i.d.) to investigate whether efficacy could be observed. Female NMRI mice ($n = 5$ per dose group) were infected with *T. b. brucei* GVR35 (inoculum 1×10^4 parasites), and treatment commenced with **63** at 100 mg/kg po b.i.d. on day 21 postinfection for 5 days. No difference in survival time from that of vehicle control animals was observed. In contrast, melarsoprol (20 mg/kg ip once daily for 5 days), as positive control, was fully curative (100% survival to 180 days postinfection).

In terms of developability, the hepatic microsomal intrinsic clearance in rat ($0.5 \text{ mL min}^{-1} \text{ g}^{-1}$) and human ($1.2 \text{ mL min}^{-1} \text{ g}^{-1}$) is similar to that observed in mouse ($0.6 \text{ mL min}^{-1} \text{ g}^{-1}$), suggesting that blood clearance in these species should not be too dissimilar from that observed in mouse. Compound **63** does not have a significant hERG liability (IC₅₀ = 28 μM; automated patch clamp) and no significant drug–drug interaction liability ($\leq 10\%$ inhibition at 1 μM across the five

Table 5. Activities of Constrained Analogues against *Tb*NMT, *Hs*NMT-1, and *T. brucei*^a

									
No.	R	<i>Tb</i> NMT IC ₅₀ (μM)	<i>Hs</i> NMT-1 IC ₅₀ (μM)	<i>T. brucei</i> EC ₅₀ (μM)	No.	R	<i>Tb</i> NMT IC ₅₀ (μM)	<i>Hs</i> NMT-1 IC ₅₀ (μM)	<i>T. brucei</i> EC ₅₀ (μM)
56		49	>100	n.d.	60		4.3	4.3	n.d.
57		1.2	4.2	3.6	61		0.005	0.007	0.013
58		11	45	n.d.	62		0.02	0.12	0.13
59		0.29	0.75	1.1	63		0.002	0.003	0.002

^aIC₅₀ values are shown as mean values of two or more determinations. Standard deviation is typically within 2-fold from the IC₅₀.

Scheme 5^a

^aReagents: (i) B(OH)₂R or B(OR)₂R, K₃PO₄, DMF, H₂O, Pd(dppf)Cl₂·DCM; (ii) bis-pinacolatodiboron, K₃PO₄, THF, Pd(PPh₃)₄; (iii) RBr, K₃PO₄, DMF, H₂O, Pd(PPh₃)₄; (iv) HNR₂, NaBH(OAc)₃, CHCl₃.

major human isoforms CYP1A2, CYP2C9, CYP2C19, CYP2D6, and CYP3A4) and therefore represents an exciting druggable lead for further development of a stage 1 compound for treatment of HAT.

Structural Studies. Attempts to crystallize the *Tb*NMT have been unsuccessful to date. However, during the course of this project, we were able to obtain a structure for *Leishmania major* NMT (*Lm*NMT), which we have used as a surrogate

model for *Tb*NMT. To further understand and confirm the SAR, we have carried out a retrospective structural analysis of selected ligands. This shows that **1**, **29**, **42**, **59**, and **63** occupy the substrate binding groove of *Lm*NMT (Figure 3A). The pyrazole moieties superimpose well, occupying a pocket formed predominantly by the side chains of Val81, Asp83, Phe88, Phe90, Phe232, Ser330, Leu341, and Tyr345 that bind residues 4 and 5 of the peptide substrate (Figure 3B). This pocket has

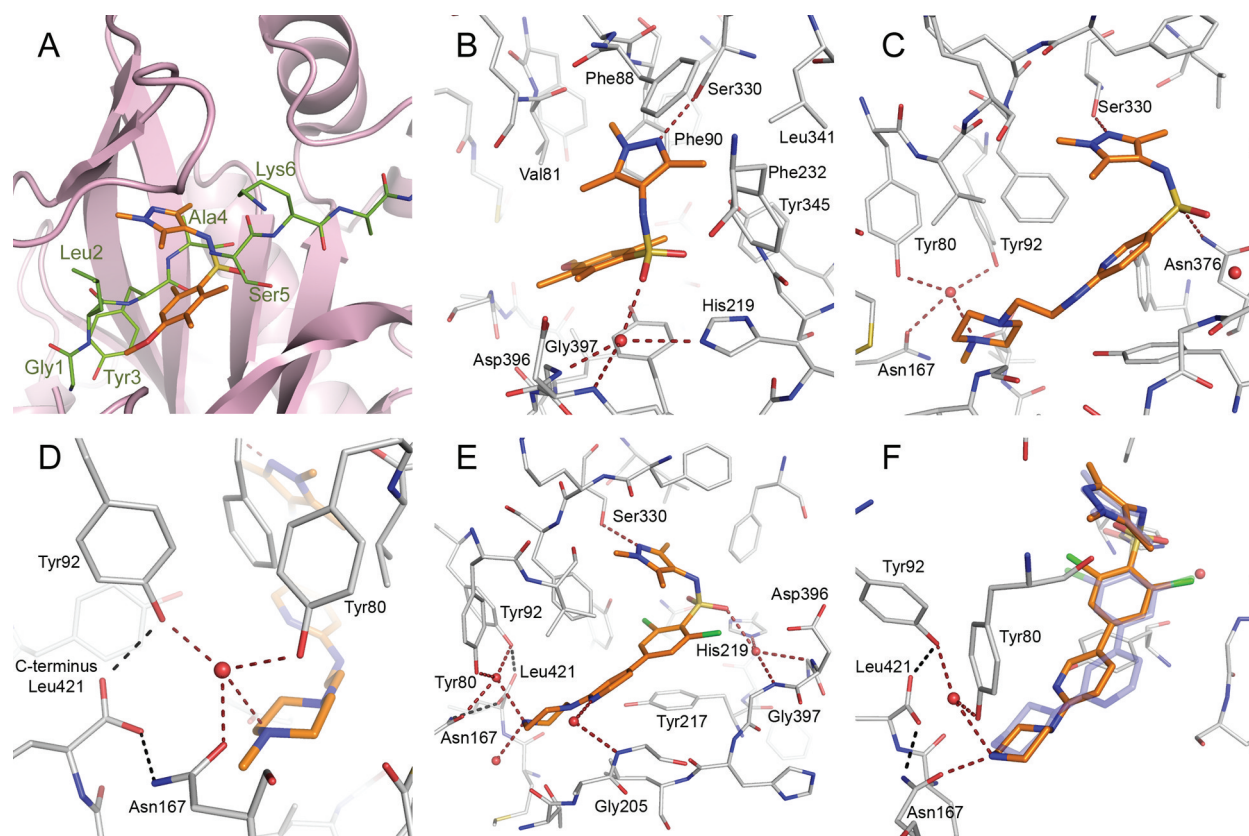


Figure 3. Structural analysis of the pyrazole sulfonamide inhibitors of NMT. Panel A shows the binding mode of screening hit **1** bound to *Lm*NMT (gold C atoms) overlaid with the peptide GLYASKLA bound to *Sc*NMT (PDB code 1IID, green C atoms). Panels B–F show the binding modes of ligands (gold C atoms) bound to *Lm*NMT (gray C atoms). Key water molecules are shown as red spheres and hydrogen bonds as dashed lines. Key residues are labeled for clarity. Panel B shows the binding mode of **1** forming canonical interactions formed by pyrazole sulfonamide moieties. Panel C shows the binding mode of **42** extending down toward the C-terminus, picking up water mediated interactions close to the terminal carboxylate. Panel D shows in detail the hydrogen bonding interactions of the conserved hydration site around the C-terminus and the interaction with the methylpiperazine of **42**. Panel E shows the binding mode of the highly potent molecule **63** (PDB code 2WSA). Panel F shows the binding mode of the para-substituted molecule **59** (gold C atoms) overlaid with the binding mode of the meta-substituted **63** (purple C atoms, partially transparent). This illustrates the strained conformation of **59** and the altered hydrogen bonding pattern of the piperazine moiety.

not been exploited in previously reported series of NMT inhibitors developed against the *C. albicans* and *Saccharomyces cerevisiae* enzymes because this pocket does not exist in these two species. Instead of a serine, there is a phenylalanine that occupies the same space as the pyrazole group of our ligands. In *Lm*NMT the pyrazole nitrogen lone pair forms a hydrogen bond with the side chain hydroxyl group of Ser330. The pyrazole *N*-methyl group interacts with the side chains of Val81 and the aromatic ring of Phe90. As seen from the SAR, substituents larger than methyl at this nitrogen are not tolerated because of the steric constraints exerted by this pocket. The methyl in the 3-position of the pyrazole is packed against the aromatic group of Phe88 and the side chain of Leu341. Subsequent SAR studies (to be reported in due course) have shown that this interaction provides an important contribution to binding.

The sulfonamide moiety of **1**, **59**, and **63** hydrogen-bonds through a highly coordinated water molecule to the side chain of His219 and the backbone amides of Asp396 and Gly397. This water molecule mimics the side chain hydroxyl of a Ser/Thr residue, an important feature of the consensus sequence at position 5 of the substrate peptide. There is a degree of flexibility in the position and orientation of the sulfonamide group; in **29** this moiety sits 0.8 Å closer to the Asn376-His219 pair and the water mediated hydrogen bonds are retained

(Supporting Information, Table S6). In **42** the hydrogen bonding pattern of the sulfonamide is altered with the water bridged interaction with His219 being replaced by a direct contact between the sulfonamide oxygen and the side chain of Asn376. This tendency for the sulfonamide to occupy various positions makes it difficult to rationalize the exact importance of its binding contribution, and we suggest that this group may indeed only be important for optimal disposition of the pyrazole relative to the central aromatic. The benzene rings of **1**, **29**, **59**, and **63** do not form directional interactions with the protein, though they stack above the side chain of Tyr217, which lines the floor of the peptide binding site. Hydrophobic packing is increased further by the two chlorine atoms of **63**, explaining their beneficial effect on potency. In **42**, the pyridyl nitrogen of this core ring potentially forms a water bridged interaction with the side chains of Tyr345 and Tyr217 with the linker nitrogen atom forming a water bridged interaction with the backbone carbonyl of His398.

As previously observed, the presence of a basic functionality near the C-terminal carboxylate results in large gains in potency. However, in contrast to the Roche benzofuran that interacts directly with the carboxylate group (PDB code 1IYL), the series described here hydrogen-bond indirectly to the C-terminal carboxylate via a network of water molecules (Figure 3C and Figure 3D). The residues that form this hydration site

are all fully conserved throughout all NMTs. The alkyl chain of **42** extends down the peptide binding groove, allowing the methylated nitrogen of the piperazine to hydrogen bond with a water network formed by the side chains of Tyr92 and Asn167. An additional hydrogen bond is formed between the water molecule and the phenolic hydroxyl of Tyr80. The most potent inhibitor **63** presents the terminal piperazine nitrogen 2.8 Å from a tightly bound water molecule, and an additional hydrogen bond is made with another water network close to Met420. An additional water mediated hydrogen bond is formed between the pyridyl nitrogen atom and the amide of Gly205 (Figure 3E).

Comparison of the binding modes of **63** and its para-substituted counterpart **59** provides some insight into the large potency difference between the two molecules, despite retaining the pyrazole, sulfonamide, and to some extent the piperazine interactions (Figure 3F). The piperazine moiety of **63** forms two strong hydrogen bonds with excellent geometry to the solvent network around the C-terminal carboxylate. In the case of **59** two potential hydrogen bonds can be fulfilled, first to the well conserved water molecule described for **42** and to the side chain carbonyl of Asn167; however, the geometry of these interactions is suboptimal with the stronger of the two hydrogen bonds formed directly to the asparagine side chain. The meta-substitution of **63** allows the molecule to access a greater range of spatial orientations as opposed to the linear para-substitution of **59** which results in a strained conformation within the active site, suggesting that entropic constraints play a significant role in binding. The reduced enzyme activity of the para-substituted molecules may be attributed to a combination of the steric constraint and the suboptimal hydrogen bonding network around the C-terminal carboxylate.

CONCLUSION

Chemistry-driven optimization of a screening hit has resulted in the discovery of pyrazolesulfonamide DDD85646 (**63**), a highly potent, trypanocidal, orally active prototype inhibitor of *Tb*NMT, which cures rodents of systemic infection with *T. b. brucei* and *T. b. rhodesiense* strains. As previously reported, a number of biological studies have already established that **63** acts on target:¹⁷ (i) overexpression of *Tb*NMT in *T. brucei* (5-fold) led to a reduced sensitivity to **63** (8-fold); (ii) incubation of the parasites with **63** prevented incorporation of radiolabeled myristoyl-CoA into proteins; (iii) more generally over the series, there was a good correlation between inhibition of the enzyme and inhibition of parasite growth in culture. The precise mechanism by which inhibition of NMT causes its antiparasitic effects is not known. However, we suggest that a pleiotropic effect, caused by the inhibition of myristoylation of multiple important substrates, accounts for the effectiveness of **63** in cell culture and in vivo.

Although during this program we did not have structural information to guide inhibitor design, we are presently able to rationalize SAR using the structural information gained from surrogate crystallography in *Lm*NMT. The majority of residues lining the active site are conserved between the *T. brucei* and human NMT enzymes, which may explain why many of the inhibitors including **63** show little selectivity. In the absence of a structure of *Tb*NMT, we are unable to delineate useful differences between *Hs*NMT and *Tb*NMT that could inform the design of selective inhibitors. However, compounds within this series, such as **42**, can possess a promising level of selectivity.

We have discovered a useful prototype inhibitor of *Tb*NMT that is trypanocidal, has good oral pharmacokinetics, and is effective in acute models of disease, thus allowing us to successfully validate *Tb*NMT as a target for drug discovery. The limitations of **63**, its inability to cross the blood–brain barrier and lack of selectivity against *Hs*NMT, are clearly factors that need to be addressed. Work is currently ongoing to optimize the selectivity and pharmacokinetic properties of compounds within this series to identify potential clinical candidates that can deliver an efficacious free concentration in the brain at a well-tolerated dose.

EXPERIMENTAL SECTION

General Experimental Information. Chemicals and solvents were purchased from Aldrich Chemical Co., Fluka, ABCR, VWR, Acros, Fisher Chemicals, and Alfa Aesar and were used as received unless otherwise stated. Air- and moisture-sensitive reactions were carried out under an inert atmosphere of argon in oven-dried glassware. Analytical thin-layer chromatography (TLC) was performed on precoated TLC plates (layer 0.20 mm silica gel 60 with fluorescent indicator UV254, from Merck). Developed plates were air-dried and analyzed under a UV lamp (UV 254/365 nm). Flash column chromatography was performed using prepacked silica gel cartridges (230–400 mesh, 40–63 μm, from SiliCycle) using a Teledyne ISCO Combiflash Companion or Combiflash Retrieve. ¹H NMR and ¹³C NMR spectra were recorded on a Bruker Avance II 500 spectrometer (¹H at 500.1 MHz, ¹³C at 125.8 MHz) or a Bruker DPX300 spectrometer (¹H at 300.1 MHz). Chemical shifts (δ) are expressed in ppm recorded using the residual solvent as the internal reference in all cases. Signal splitting patterns are described as singlet (s), doublet (d), triplet (t), quartet (q), pentet (p), multiplet (m), broad (br), or a combination thereof. Coupling constants (J) are quoted to the nearest 0.1 Hz. LC–MS analyses were performed with either an Agilent HPLC 1100 series connected to a Bruker Daltonics MicrOTOF or an Agilent Technologies 1200 series HPLC connected to an Agilent Technologies 6130 quadrupole spectrometer, where both instruments were connected to an Agilent diode array detector. LC–MS chromatographic separations were conducted with a Waters Xbridge C18 column, 50 mm × 2.1 mm, 3.5 μm particle size; mobile phase, water/acetonitrile + 0.1% HCOOH, or water/acetonitrile + 0.1% NH₃; linear gradient from 80:20 to 5:95 over 3.5 min and then held for 1.5 min; flow rate of 0.5 mL min⁻¹. All assay compounds had a measured purity of ≥95% (by TIC and UV) as determined using this analytical LC–MS system. High resolution electrospray measurements were performed on a Bruker Daltonics MicrOTOF mass spectrometer. Microwave-assisted chemistry was performed using a Biotage initiator microwave synthesizer. Compounds **25**, **26**, **33**, and **34** were purchased from Enamine as solids. Purity (>97%) and molecular mass were confirmed by HPLC and high resolution mass spectrometry.

Prototypical Procedure for Preparation of a Sulfonamide from an Amine and a Sulfonyl Chloride. 4-Methoxy-2,3,6-trimethyl-N-(1,3,5-trimethyl-1H-pyrazol-4-yl)benzenesulfonamide (**1**). 4-Methoxy-2,3,6-trimethylbenzenesulfonyl chloride (500 mg, 2.0 mmol) was added portionwise to a stirred solution of 4-amino-1,3,5-trimethyl-1H-pyrazole (250 mg, 2.0 mmol) in pyridine (10.0 mL) at room temperature. The mixture was stirred for 24 h and then concentrated to dryness in vacuo. The resulting residue was diluted with DCM and washed with saturated aqueous NaHCO₃. The organic phase was separated, dried (MgSO₄), filtered, and concentrated to dryness in vacuo. Trituration from Et₂O and collection by vacuum filtration gave the title compound **1** as a fine off-white solid (380 mg, 1.13 mmol, 57%). ¹H NMR (500 MHz, DMSO-*d*₆): δ 8.87 (s, 1H), 6.67 (s, 1H), 3.48 (s, 3H), 3.28 (s, 3H), 2.33 (s, 3H), 2.21 (s, 3H), 2.01 (s, 3H), 1.77 (s, 3H), 1.54 (s, 3H). HRMS (*m/z*): [MH⁺] calcd for C₁₆H₂₄N₃SO₃, 338.1533; found 338.1533.

4-Bromo-2,6-dichloro-N-(1,3,5-trimethyl-1H-pyrazol-4-yl)benzenesulfonamide (**29**).¹⁷ Compound **29** was prepared from 4-bromo-2,6-dichlorobenzenesulfonyl chloride (5.0 g, 15.4 mmol) and 4-amino-1,3,5-trimethyl-1H-pyrazole (1.93 g, 15.4 mmol) in pyridine

(35.0 mL) according to the method of 1, to give the title compound 29 as an off-white solid (5.64 g, 13.7 mmol, 89%). ¹H NMR (300 MHz, DMSO-*d*₆): δ 9.75 (s, 1H), 8.00 (s, 2H), 3.57 (s, 3H), 1.93 (s, 3H), 1.72 (s, 3H). HRMS (*m/z*): [MH⁺] calcd for C₁₂H₁₃N₃SO₂Cl₂Br, 411.9283; found 411.9282.

6-Chloropyridine-3-sulfonic Acid (1,3,5-Trimethyl-1H-pyrazol-4-yl)amide (37). 37 was prepared from 6-chloropyridine-3-sulfonyl chloride (4.8 g, 22.7 mmol) and 4-amino-1,3,5-trimethyl-1H-pyrazole (2.84 g, 22.7 mmol) in pyridine (35.0 mL) according to the method of 1, to give the title compound 37 as an off-white solid (5.13 g, 17.1 mmol, 75%). ¹H NMR (500 MHz, DMSO-*d*₆): δ 9.51 (s, 1H), 8.59 (d, *J* = 2.3 Hz, 1H), 8.03 (dd, *J* = 7.6 Hz, 2.3 Hz, 1H), 7.77 (d, *J* = 7.6 Hz, 1H), 3.58 (s, 3H), 1.84 (s, 3H), 1.63 (s, 3H). HRMS (*m/z*): [MH⁺] calcd for C₁₁H₁₄N₄SO₂Cl, 301.0521; found 301.0523.

Prototypical Procedure for N-Alkylation of Compound 2. *N*-(1-Propyl-3,5-dimethyl-1H-pyrazol-4-yl)-4-methoxy-2,3,6-trimethylbenzenesulfonamide (3). A solution of *N*-(3,5-dimethyl-1H-pyrazol-4-yl)-4-methoxy-2,3,6-trimethylbenzenesulfonamide 2 (100 mg, 0.31 mmol), cesium carbonate (202 mg, 0.62 mmol), and 1-bromopropane (76 mg, 0.62 mmol) in DMF (10.0 mL) was heated to 80 °C for 1 h in a microwave. The mixture was partitioned between ethyl acetate (25 mL) and brine (25 mL), dried (MgSO₄), filtered, and concentrated to dryness in vacuo. The resulting residue was purified by column chromatography (SiO₂, 1:1 ethyl acetate/hexane) to give the title compound as an off-white solid (27 mg, 0.07 mmol, 24%). ¹H NMR (500 MHz, DMSO-*d*₆): δ 8.67 (s, 1H), 6.45 (s, 1H), 4.46 (t, *J* = 6.9 Hz, 2H), 3.78 (s, 3H), 2.58 (s, 3H), 2.36 (s, 3H), 2.16 (s, 3H), 2.04 (s, 3H), 1.98 (m, 2H), 1.83 (s, 3H), 1.21 (t, *J* = 6.9 Hz, 3H). HRMS (*m/z*): [MH⁺] calcd for C₁₈H₂₈N₃SO₃, 366.1846; found 366.1847.

Prototypical Procedure for Preparation of a 2-Aminopyridine by S_NAr Reaction of 2-Chloropyridine (37) with an Alkylamine. 6-[2-(4-Methylpiperazin-1-yl)ethylamino]pyridine-3-sulfonic Acid (1,3,5-Trimethyl-1H-pyrazol-4-yl)amide (42). 6-Chloro-*N*-(1,3,5-trimethyl-1H-pyrazol-4-yl)pyridine-3-sulfonamide (37) (225 mg, 0.75 mmol) and 4-(2-aminoethyl)methylpiperazine (215 mg, 1.5 mmol) in ethanol (2.0 mL) were heated at 155 °C for 1 h by microwave in a sealed vessel. Dilution with DCM (25 mL), washing with saturated aqueous sodium hydrogen carbonate solution (2 × 5 mL), drying (MgSO₄), and concentration in vacuo gave a residual oil which was subjected to chromatography (SiO₂, 10:90 MeOH/EtOAc) to give the title compound as an off-white powder (198 mg, 0.49 mmol, 65%). ¹H NMR (300 MHz, DMSO-*d*₆): δ 8.77 (s, 1H), 8.07 (d, *J* = 2.2 Hz, 1H), 7.45 (dd, *J* = 2.2 Hz, 8.9 Hz, 1H), 7.28 (s br, 1H), 6.54 (d, *J* = 8.9 Hz, 1H), 3.57 (s, 3H), 3.44–3.39 (m, 2H), 2.41 (t, *J* = 6.1 Hz, 2H), 2.41 (s br, 4H), 2.36–2.31 (s br, 4H and 3H), 2.16 (s, 3H), 1.89 (s, 3H), 1.67 (s, 3H). HRMS (*m/z*): [MH⁺] calcd for C₁₈H₃₀N₇SO₂, 408.2176; found 408.2185.

Prototypical Procedure for the Suzuki Reaction between an Aryl Bromide and a Boronic Acid/Boronate Ester. 2,6-Dichloro-4-(2-piperazin-1-ylpyridin-4-yl)-*N*-(1,3,5-trimethyl-1H-pyrazol-4-yl)benzenesulfonamide (63).¹⁷ A deoxygenated solution of 4-bromo-2,6-dichloro-*N*-(1,3,5-trimethyl-1H-pyrazol-4-yl)benzenesulfonamide (29) (13.84 g, 33.3 mmol), 2-(1-piperazinyl)pyridine-4-boronic acid pinacol ester (11.57 g, 40.0 mmol), tribasic potassium phosphate (9.73 g, 44.0 mmol), and Pd(PPh₃)₄ (1.50 g, 0.96 mmol) in DMF (200 mL) and water (40 mL) in a round-bottomed flask under argon was heated at 120 °C for 1 h. The reaction mixture was then concentrated in vacuo, diluted with DCM (400 mL), washed with saturated aqueous ammonia solution (2 × 100 mL), dried (MgSO₄), and concentrated in vacuo. The residual solid was triturated from Et₂O and collected by filtration to give a solid which was recrystallized from EtOAc to give the title compound 63 as an off-white powder (15.22 g, 30.7 mmol, 92%). ¹H NMR (500 MHz, DMSO-*d*₆): δ 9.79 (s, 1H), 8.25 (d, *J* = 5.9 Hz, 1H), 8.20 (s, 2H), 7.61 (s, 1H), 7.40 (d, *J* = 5.9 Hz, 1H), 4.08 (s br, 4H), 3.63 (s, 3H), 3.28 (s br, 4H), 2.00 (s, 3H), 1.77 (s, 3H). ¹³C NMR (125 MHz, DMSO-*d*₆): 147.5, 147.3, 143.8, 137.4, 136.3, 135.2, 129.8, 111.8, 111.7, 109.1, 108.9, 42.7, 42.0, 36.2, 10.4. HRMS (*m/z*): [MH⁺] calcd for C₂₁H₂₅N₆SO₂Cl₂, 495.1131; found 495.1124.

Enzyme Inhibition Assay. *N*-Myristoyltransferase is an enzyme that catalyzes the addition of myristic acid from myristoyl-CoA to the N-terminal glycine residue of numerous substrate proteins and peptides with the subsequent release of coenzyme A. ³H-labeled myristoyl-CoA (GE Healthcare) can be used in the reaction to transfer ³H-myristic acid to a biotinylated substrate peptide (GCGGSKVKPQ-PPQAK(biotin)-amide, Pepceuticals Inc.). The reaction can be measured by the subsequent binding of the labeled peptide to streptavidin-coated scintillation proximity assay (SPA) beads (GE Healthcare) and monitoring of β-particle excitation of the embedded scintillant (Figure 1).

Measurement of the ability of compounds to inhibit the *N*-myristoyltransferase enzyme(s) of human (*HsNMT-1* and *HsNMT-2*) and kinetoplast (*T. brucei*, *T. cruzi*, and *L. major*) species was performed using a modification of the scintillation proximity assay platform described previously by Panethymitaki et al.²⁰ as follows: Compounds were solubilized in DMSO at a top concentration of 10 mM and serially diluted in half log steps to achieve a range of final assay concentrations of 100 μM to 1.5 nM. Compound at each concentration was added to white 384-well plates in a volume of 0.5 μL. *N*-Myristoyltransferase enzyme (*HsNMT-1*, *HsNMT-2*, *TcNMT*, *TbNMT*, or *LmNMT*), dissolved to a working concentration of 10 nM in assay buffer (30 mM Tris-HCl, pH 7.4, 0.5 mM EGTA, 0.5 mM EDTA, 1.25 mM DTT, 0.1% Triton X-100), was then added to columns 1–11 and 13–23 of the plates in a volume of 20 μL. To columns 12 and 24, 20 μL of assay buffer was added to provide a no enzyme control. Following a 5 min incubation at room temperature the substrates (GCGGSKVKPQPPQAK(biotin)-amide and myristoyl-CoA), dissolved in assay buffer, were added to all wells in a volume of 20 μL to start the reaction. The final concentrations of peptide and ³H-myristoyl-CoA were 0.5 μM and 125 nM, respectively, and the specific activity of the radiolabel was 8 Ci/mmol. Plates were then incubated at room temperature for up to 50 min (dependent upon the period of linearity for the different enzyme species) before SPA beads, suspended to 1 mg/mL in a stop solution (200 mM phosphoric acid/NaOH, pH 4, 750 mM MgCl₂), were added in a volume of 40 μL. Plates were then read on a TopCount microplate luminometer and data analyzed by calculating the percentage inhibition compared to the maximum and minimum assay controls. Concentration effect curves were fitted using nonlinear regression using XLFit 4.2, and IC₅₀ values were determined.

Cell Viability Assay. Measurement of the ability of the compounds to inhibit human (MRC5, human lung fibroblast cells) and trypanosome (*T. b. brucei*, BSF427, VSG118) cell growth was performed using a modification of the cell viability assay previously described by Raz et al.²⁹ Compounds were dissolved in DMSO at a top concentration of 10 mM and serially diluted in half log steps to achieve a range of final assay concentrations of 50 μM to 0.5 nM. Compound at each concentration (200-fold final) was added to clear 96-well tissue culture plates in a volume of 1 μL. Then 2000 cells per well in relevant growth medium (HMI-9T for *T. brucei*, a modification of HMI-9 as described by Hurumi et al.,³⁰ where 0.2 mM 2-mercaptoethanol was replaced with 0.056 mM thiolglycerol, and MEM with 10% FBS for MRC5) were then added to columns 1–11 of the plates in a volume of 199 μL. To column 12, 200 μL of medium was added to provide a no cells control. Plates were then incubated at 37 °C in an atmosphere of 5% CO₂ for 69 h, before the addition of 20 μL of 500 μM rezasurin solution, and a further incubation period of 4 h. Plates were then read on a BioTek flx800 fluorescent plate reader, and percentage inhibition was compared to the maximum and minimum assay controls. Concentration effect curves were fitted using nonlinear regression using XLFit 4.2 and EC₅₀ values determined.

Crystallography. The expression construct for 6xHis-TEV site, *LmNMT* (5-421), was obtained from the Structural Genomics Consortium (SGC), Toronto, Canada. The protein was expressed in *E. coli* Rosetta (DE3) using autoinduction medium. Cells were harvested by centrifugation and resuspended in 50 mM HEPES, pH 7.5, 0.5 M NaCl, 5 mM imidazole, 5% glycerol (plus DNase, lysozyme, and a protease inhibitor cocktail) and lysed by passage through a constant cell disruptor (Constant Cell Systems). Chromatography steps were carried out using an AKTA system

(GE Healthcare). The lysate was cleared by centrifugation (50K rcf 30 min) and loaded onto a 5 mL HisTRAP crude column (GE Healthcare), and target protein was eluted by a 5–250 mM imidazole gradient. Fractions containing *LmNMT* were pooled, desalted, and applied to a 6 mL Resource-Q column pre-equilibrated with 10 mM HEPES, pH 7.5. *LmNMT* was eluted by 0–500 mM NaCl gradient, and fractions were analyzed by SDS–PAGE with fractions greater than 95% purity concentrated to 9 mg/mL for crystallization.

Crystals of *LmNMT* with myristoyl-CoA were obtained by incubating the protein with 1 mM myristoyl-CoA for 1 h at 4 °C prior to crystallization. Protein crystals were obtained via the hanging drop vapor diffusion method by mixing 2 μ L of protein solution mixed with 2 μ L of reservoir solution that consisted of 24–30% PEG1500, 0.2 M NaCl, and 0.1 M Na cacodylate, pH 5.6. Rod shaped crystals appeared after 2–4 days at 20 °C.

Protein–ligand complexes were obtained by soaking the crystals for 16 h in mother liquor derived cryoprotectant (25% PEG1500, 0.2 M NaCl, 0.1 M Na cacodylate, pH 5.6, 20% glycerol) + 15 mM ligand, prepared from a stock concentration of 0.2 M in DMSO. Crystals were flash frozen in liquid nitrogen and stored before data measurement. X-ray diffraction data were measured at the ESRF using beamlines ID-29 and ID23-2 and the data reduced using the HKL suite.³¹ Molecular replacement was carried out using MOLREP³² with the binary *LmNMT* + myristoyl-CoA structure (PDB code 3HSZ) used as a search model. The models were refined using REFMAC5,³³ and manual alteration was carried out using COOT³⁴ with ligand coordinate and topology files created with PRODRG.³⁵ Coordinates and associated diffraction data for complexes of *LmNMT* + **1**, **29**, **42**, **62**, and **59** have been deposited in the Protein Data Bank (PDB) with accession codes 4A2Z, 4A30, 4A31, 4A32, and 4A33, respectively.

■ ASSOCIATED CONTENT

● Supporting Information

Synthetic details for all compounds, additional compound biological data (Tables S1–S4), and X-ray crystallographic data (Tables S5 and S6). This material is available free of charge via the Internet at <http://pubs.acs.org>.

■ AUTHOR INFORMATION

Corresponding Author

*Phone: +44 1382 386 240. E-mail: i.h.gilbert@dundee.ac.uk.

■ ACKNOWLEDGMENTS

Funding for this work was provided by the Wellcome Trust (Grants WT077705, WT083481, WT085622). The authors thank Gina McKay for performing HRMS analyses and for assistance with performing other NMR and MS analyses, Daniel James for data management, Bhavya Rao for performing parasite assays, Dr. Gian-Fillipo Ruda for synthesis of RO-09-4879, and Dr. Stephen Patterson for critical evaluation of the manuscript.

■ ABBREVIATIONS USED

NMT, *N*-myristoyltransferase; HAT, human African trypanosomiasis; ARF-1, ADP-ribosylation factor-1 protein; ARL-1, ADP-ribosylation factor-like protein; HTS, high throughput screen; CAP5.5, cytoskeleton associated protein 5.5; SPA, scintillation proximity assay; PSA, polar surface area; NMRI, Naval Medical Research Institute; CYP, cytochrome P450; hERG, human ether-a-go-go-related gene; PDB, Protein Data Bank

■ REFERENCES

- (1) Jacobs, R. T.; Nare, B.; Phillips, M. A. State of the art in African trypanosome drug discovery. *Curr. Top. Med. Chem.* **2011**, *11*, 1255–1274.
- (2) Bowyer, P. W.; Tate, E. W.; Leatherbarrow, R. J.; Holder, A. A.; Smith, D. F.; Brown, K. A. *N*-Myristoyltransferase: a prospective drug target for protozoan parasites. *ChemMedChem* **2008**, *3*, 402–408.
- (3) Price, H. P.; Guthrie, M. L. S.; Ferguson, M. A. J.; Smith, D. F. Myristoyl-CoA:protein *N*-myristoyltransferase depletion in trypanosomes causes avirulence and endocytic defects. *Mol. Biochem. Parasitol.* **2010**, *169*, 55–58.
- (4) Gelb, M. H.; Van Voorhis, W. C.; Buckner, F. S.; Yokoyama, K.; Eastman, R.; Carpenter, E. P.; Panethymitaki, C.; Brown, K. A.; Smith, D. F. Protein farnesyl and *N*-myristoyl transferases: piggy-back medicinal chemistry targets for the development of antitrypanosomatid and antimalarial therapeutics. *Mol. Biochem. Parasitol.* **2003**, *126*, 155–163.
- (5) Price, H. P.; Goulding, D.; Smith, D. F. ARL1 has an essential role in *Trypanosoma brucei*. *Biochem. Soc. Trans.* **2005**, *33*, 643–645.
- (6) Brown, D. L.; Devadas, B.; Lu, H. F.; Nagarajan, S.; Zupec, M. E.; Freeman, S. K.; McWherter, C. A.; Getman, D. P.; Sikorski, J. A. Replacements for lysine in L-seryl-L-lysyl dipeptide amide inhibitors of *Candida albicans* myristoyl-CoA:protein *N*-myristoyltransferase. *Bioorg. Med. Chem. Lett.* **1997**, *7*, 379–382.
- (7) Devadas, B.; Freeman, S. K.; Zupec, M. E.; Lu, H. F.; Nagarajan, S. R.; Kishore, N. S.; Lodge, J. K.; Kuneman, D. W.; McWherter, C. A.; Vinjamoori, D. V.; Getman, D. P.; Gordon, J. I.; Sikorski, J. A. Design and synthesis of novel imidazole-substituted dipeptide amides as potent and selective inhibitors of *Candida albicans* myristoylCoA:protein *N*-myristoyltransferase and identification of related tripeptide inhibitors with mechanism-based antifungal activity. *J. Med. Chem.* **1997**, *40*, 2609–2625.
- (8) Devadas, B.; Zupec, M. E.; Freeman, S. K.; Brown, D. L.; Nagarajan, S.; Sikorski, J. A.; McWherter, C. A.; Getman, D. P.; Gordon, J. I. Design and syntheses of potent and selective dipeptide inhibitors of *Candida albicans* myristoyl-CoA:protein *N*-myristoyltransferase. *J. Med. Chem.* **1995**, *38*, 1837–1840.
- (9) Nagarajan, S. R.; Devadas, B.; Zupec, M. E.; Freeman, S. K.; Brown, D. L.; Lu, H. F.; Mehta, P. P.; Kishore, N. S.; McWherter, C. A.; Getman, D. P.; Gordon, J. I.; Sikorski, J. A. Conformationally constrained [*p*-(omega-aminoalkyl)phenacetyl]-L-seryl-L-lysyl dipeptide amides as potent peptidomimetic inhibitors of *Candida albicans* and human myristoyl-CoA:protein *N*-myristoyl transferase. *J. Med. Chem.* **1997**, *40*, 1422–1438.
- (10) Sikorski, J. A.; Devadas, B.; Zupec, M. E.; Freeman, S. K.; Brown, D. L.; Lu, H. F.; Nagarajan, S.; Mehta, P. P.; Wade, A. C.; Kishore, N. S.; Bryant, M. L.; Getman, D. P.; McWherter, C. A.; Gordon, J. I. Selective peptidic and peptidomimetic inhibitors of *Candida albicans* myristoylCoA:protein *N*-myristoyltransferase: a new approach to antifungal therapy. *Biopolymers* **1997**, *43*, 43–71.
- (11) Ebiike, H.; Masubuchi, M.; Liu, P. L.; Kawasaki, K.; Morikami, K.; Sogabe, S.; Hayase, M.; Fujii, T.; Sakata, K.; Shindoh, H.; Shiratori, Y.; Aoki, Y.; Ohtsuka, T.; Shimma, N. Design and synthesis of novel benzofurans as a new class of antifungal agents targeting fungal *N*-myristoyltransferase. Part 2. *Bioorg. Med. Chem. Lett.* **2002**, *12*, 607–610.
- (12) Kawasaki, K.; Masubuchi, M.; Morikami, K.; Sogabe, S.; Aoyama, T.; Ebiike, H.; Niizuma, S.; Hayase, M.; Fujii, T.; Sakata, K.; Shindoh, H.; Shiratori, Y.; Aoki, Y.; Ohtsuka, T.; Shimma, N. Design and synthesis of novel benzofurans as a new class of antifungal agents targeting fungal *N*-myristoyltransferase. Part 3. *Bioorg. Med. Chem. Lett.* **2003**, *13*, 87–91.
- (13) Masubuchi, M.; Ebiike, H.; Kawasaki, E.; Sogabe, S.; Morikami, K.; Shiratori, Y.; Tsujii, S.; Fujii, T.; Sakata, K.; Hayase, M.; Shindoh, H.; Aoki, Y.; Ohtsuka, T.; Shimma, N. Synthesis and biological activities of benzofuran antifungal agents targeting fungal *N*-myristoyltransferase. *Bioorg. Med. Chem.* **2003**, *11*, 4463–4478.
- (14) Masubuchi, M.; Kawasaki, K.; Ebiike, H.; Ikeda, Y.; Tsujii, S.; Sogabe, S.; Fujii, T.; Sakata, K.; Shiratori, Y.; Aoki, Y.; Ohtsuka, T.;

Shimma, N. Design and synthesis of novel benzofurans as a new class of antifungal agents targeting fungal *N*-myristoyltransferase. Part 1. *Bioorg. Med. Chem. Lett.* **2001**, *11*, 1833–1837.

(15) Ebara, S.; Naito, H.; Nakazawa, K.; Ishii, F.; Nakamura, M. FTR1335 is a novel synthetic inhibitor of *Candida albicans* *N*-myristoyltransferase with fungicidal activity. *Biol. Pharm. Bull.* **2005**, *28*, 591–595.

(16) Yamazaki, K.; Kaneko, Y.; Suwa, K.; Ebara, S.; Nakazawa, K.; Yasuno, K. Synthesis of potent and selective inhibitors of *Candida albicans* *N*-myristoyltransferase based on the benzothiazole structure. *Bioorg. Med. Chem.* **2005**, *13*, 2509–2522.

(17) Frearson, J. A.; Brand, S.; McElroy, S. P.; Cleghorn, L. A. T.; Smid, O.; Stojanovski, L.; Price, H. P.; Guther, M. L. S.; Torrie, L. S.; Robinson, D. A.; Hallyburton, I.; Mpamhanga, C. P.; Brannigan, J. A.; Wilkinson, A. J.; Hodgkinson, M.; Hui, R.; Qiu, W.; Raimi, O. G.; Van Aalten, D. M. F.; Brenk, R.; Gilbert, I. H.; Read, K. D.; Fairlamb, A. H.; Ferguson, M. A. J.; Smith, D. F.; Wyatt, P. G. *N*-Myristoyltransferase inhibitors as new leads to treat sleeping sickness. *Nature* **2010**, *464*, 728–732.

(18) Brand, S.; Wyatt, P.; Thompson, S.; Smith, V.; Bayliss, T.; Harrison, J.; Norcross, N.; Cleghorn, L.; Gilbert, I.; Brenk, R. *N*-Myristoyl Transferase Inhibitors. WO2010026365, 2010.

(19) Frearson, J. A.; Wyatt, P. G.; Gilbert, I. H.; Fairlamb, A. H. Target assessment for antiparasitic drug discovery. *Trends Parasitol.* **2007**, *23*, 589–595.

(20) Panethymitaki, C.; Bowyer, P. W.; Price, H. P.; Leatherbarrow, R. J.; Brown, K. A.; Smith, D. F. Characterization and selective inhibition of myristoyl-CoA:protein *N*-myristoyltransferase from *Trypanosoma brucei* and *Leishmania major*. *Biochem. J.* **2006**, *396*, 277–285.

(21) Brenk, R.; Schipani, A.; James, D.; Krasowski, A.; Gilbert, I. H.; Frearson, J. A.; Wyatt, P. G. Lessons learnt from assembling screening libraries for drug discovery for neglected diseases. *ChemMedChem* **2008**, *3*, 435–444.

(22) Hertz-Fowler, C.; Ersfeld, K.; Gull, K. CAP5.5, a life-cycle-regulated, cytoskeleton-associated protein is a member of a novel family of calpain-related proteins in *Trypanosoma brucei*. *Mol. Biochem. Parasitol.* **2001**, *116*, 25–34.

(23) Hopkins, A. L.; Groom, C. R.; Alex, A. Ligand efficiency: a useful metric for lead selection. *Drug Discovery Today* **2004**, *9*, 430–431.

(24) Ebara, S.; Naito, H.; Nakazawa, K.; Ishii, F.; Nakamura, M. FTR1335 is a novel synthetic inhibitor of *Candida albicans* *N*-myristoyltransferase with fungicidal activity. *Biol. Pharm. Bull.* **2005**, *28*, 591–595.

(25) Parkin, A.; Collins, A.; Gilmore, C. J.; Wilson, C. C. Using small molecule crystal structure data to obtain information about sulfonamide conformation. *Acta Crystallogr.* **2008**, *B64*, 66–71.

(26) McWherter, C. A.; Rocque, W. J.; Zupec, M. E.; Freeman, S. K.; Brown, D. L.; Devadas, B.; Getman, D. P.; Sikorski, J. A.; Gordon, J. I. Scanning alanine mutagenesis and de-peptidization of a *Candida albicans* myristoyl-CoA:protein *N*-myristoyltransferase octapeptide substrate reveals three elements critical for molecular recognition. *J. Biol. Chem.* **1997**, *272*, 11874–11880.

(27) Maurer-Stroh, S.; Eisenhaber, B.; Eisenhaber, F. N-Terminal *N*-myristoylation of proteins: refinement of the sequence motif and its taxon-specific differences. *J. Mol. Biol.* **2002**, *317*, 523–540.

(28) Polli, J. W.; Jarrett, J. L.; Studenberg, S. D.; Humphreys, J. E.; Dennis, S. W.; Brouwer, K. R.; Woolley, J. L. Role of P-glycoprotein on the CNS disposition of amprenavir (141W94), an HIV protease inhibitor. *Pharm. Res.* **1999**, *16*, 1206–1212.

(29) Raz, B.; Iten, M.; Grether-Buhler, Y.; Kaminski, R.; Brun, R. The Alamar Blue assay to determine drug sensitivity of African trypanosomes (*T. b. rhodesiense* and *T. b. gambiense*) in vitro. *Acta Trop.* **1997**, *68*, 139–147.

(30) Hirumi, H.; Hirumi, K. Continuous cultivation of *Trypanosoma brucei* blood stream forms in a medium containing a low concentration of serum-protein without feeder cell-layers. *J. Parasitol.* **1989**, *75*, 985–989.

(31) Otwinowski, Z.; Minor, W. Processing of X-ray diffraction data collected in oscillation mode. *Methods Enzymol.* **1997**, *276*, 307–326.

(32) Vagin, A.; Teplyakov, A. An approach to multi-copy search in molecular replacement. *Acta Crystallogr. D* **2000**, *56*, 1622–1624.

(33) Murshudov, G. N.; Vagin, A. A.; Dodson, E. J. Refinement of macromolecular structures by the maximum-likelihood method. *Acta Crystallogr. D* **1997**, *53*, 240–255.

(34) Emsley, P.; Cowtan, K. Coot: model-building tools for molecular graphics. *Acta Crystallogr. D* **2004**, *60*, 2126–2132.

(35) Schuttelkopf, A. W.; van Aalten, D. M. F. PRODRG: a tool for high-throughput crystallography of protein–ligand complexes. *Acta Crystallogr. D* **2004**, *60*, 1355–1363.